Assessment of adsorptive filter for removal of formaldehyde from indoor air

Angus Shiue[a,*], Shih-Cheng Hu[a,*], Chao-Heng Tseng[b,], Cheng-Mao Chuang[b], Graham Leggett[c]**

[a] Department of Energy and Refrigerating Air-conditioning Engineering, National Taipei University of Technology, Taiwan

[b] Institute of Environment Engineering and Management, National Taipei University of Technology, Taiwan

[c] MIRICO Ltd., OX11 0QX, United Kingdom

ABSTRACT

We examine vary face velocity and initial formaldehyde concentration to investigate formaldehyde removal performance of the coconut shell activated carbon (AC) adsorptive filter media. AC surface is smooth and distributed with small pores. The surface of AC is also rather uneven, coarse and porous. Irregular layer structure were formed the amorphous. C, O, Mg, P etc. were detected, which showed the existence of MgO in AC. AC surface area is 1333.3304 m^2 g^{-1}, ketone -C=O bonds were successfully grafted on carbon. At any given face velocity, the experimental results present that adsorption capacity is increased and breakthrough time is reduced as initial concentration is increased. The breakthrough behavior of AC adsorptive filter could henceforth be investigated with confidence using the breakthrough curves predicted by the Yoon–Nelson model. Among three kinetic models, the experimental and calculated results show that the correlation coefficient and mean absolute performance error (MAPE) of Pseudo-second-order kinetic model presented the best approximation of the adsorption kinetic process dynamics than Pseudo-First Order Kinetic model and Intraparticle Diffusion model. Both of the

Intraparticle diffusion model and membrane diffusion affected the overall rate of AC adsorptive filter media adsorption process by more than one step. The equilibrium data of AC adsorptive filter media was found to best fit to the Langmuir model. The D–R equation predicted the equilibrium capacity of formaldehyde onto AC at relative pressures 0.151.

Keywords: *Adsorption; breakthrough; kinetic model; Formaldehyde*

* Denotes equal contribution

**Corresponding author:
Address: No. 1, Sec. 3, Chung Hsiao East Road, Taipei, 10608, Taiwan, Republic of China
Tel.: +886-2-27712171 ext4141
E-mail:*tsengco@ntut.edu.tw*

1. Introduction

Human beings typically spend more than 90 % of their waking hours in indoor environments. As such, pollutants found in indoor air may in many cases represent a higher hazard to human health than those present in the outdoor environment (**Brunsgaard et al. 2012**). Recent changes to Building Regulations have demanded much higher air-tightness requirements for residential and commercial buildings for reasons of improved energy conservation As a result there exists the potential for increased concentrations of volatile organic compounds (VOCs) within indoor environments. The negative impact on health and well-being and comfort (**Chuck and Kim, 2013**) of occupants in air-tight housing is well documented. Among VOCs, formaldehyde (HCHO) has long been established as a hazardous and harmful substance (**Mui et al., 2008**). The primary source of formaldehyde found as a pollutant in indoor air is pressed wood products manufactured

using urea formaldehyde resins (**U.S. Consumer Product Safety Commission, 2015**).

There are several studies on air cleaning technologies for indoor formaldehyde removal. UV photolysis is limited due to its trend to produce ozone and radicals with harmful effects. Photocatalytic oxidation has been utilized for ppm levels of contaminant degradation and ppbv concentrations need to be measured, and their main deficiencies are the short lifetime of the catalyst and the creation of harmful by-products. Cold or non-thermal plasma are not yet on the market. (**Luengas et al., 2015**) These major technical issues also have limitations like high energy consumption and low removal efficiency (**Gilbert et al., 2008, Mo et al., 2008**). Biological degradation (**Lu et al., 2012**) and botanical air filtration are still under development, currently operating at low efficiency and with insufficient understanding of long-term safety (**Luengas et al., 2015; Wang et al., 2014**). At this time, neither of these techniques is broadly employed for indoor pollutant removal (**Lu et al., 2012**). Activated carbon adsorption is a simple, effective, and low cost method to reduce the concentrations of formaldehyde removal in indoor air (**Lu et al., 2015**).

The primary purpose of this study characterized the physical and chemical properties of the AC by Scanning electron microscope (SEM), X-ray diffraction (XRD), Energy Dispersive X-Ray Spectroscopy (EDS), Brunauer–Emmett–Teller (BET), and Fourier transform infrared spectroscopy (FTIR) analysis. To investigate the equilibrium, breakthrough behavior, and the applicable assessment of three kinetic models: Pseudo-first-order, Pseudo- second-order and intraparticle diffusion. The latter assessment was conducted under various experimental conditions ,using the correlation coefficient (R^2) and the mean absolute percentage error (MAPE) to characterize the kinetic data. As a result, this study provided the essential parameters to consider when designing and operating an adsorptive purifier for removal of formaldehyde from indoor air, and implementing strategies to improve air quality in the indoor environment.

2. Materials and methods

2.1. Principle

2.1.1. Adsorptive capacity

This study used the testing method of VanOsdell et al. (**1996**) shown in **Fig. 1**. The mixed air passes through the adsorbent. Removal efficiency (η) was calculated with the initial concentration (C_0). Adsorption capacity (q_t) is defined as follow (**Shiue et al. 2010**):

$$q_t = C_0 V \int \eta(t) dt \times \frac{1}{0.082} \times \frac{1}{273+K} \times M \times 10^{-6} \qquad (1)$$

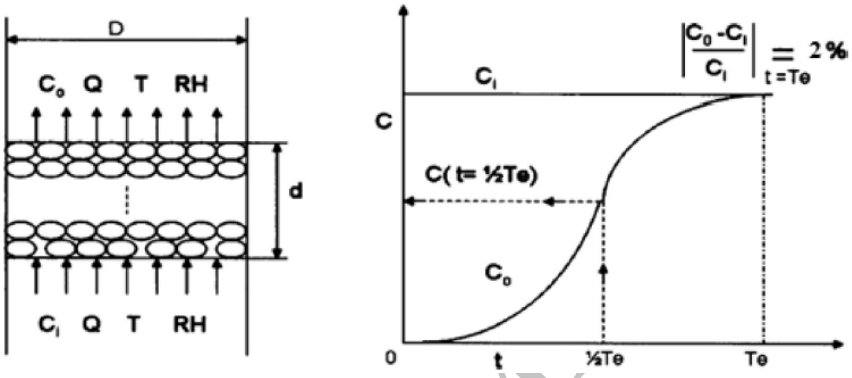

Fig. 1. Schematic diagram of testing theory

2.1.2. Breakthrough

Generally, it is not practicable to measure activated carbon filter breakthrough time against formaldehyde concentration in real indoor environments. When the outlet concentration reached 2% of the initial concentration, the breakthrough time was determined (**Dehdashti et al., 2011**). While changing only formaldehyde concentration, simplified breakthrough time estimation is shown as (**Cheng, 2008; Cheng and Tsai, 2007; Shiue et al, 2010**):

$$\frac{t_{b,1}}{t_{b,2}} = \left(\frac{C_{0,1}}{C_{0,2}}\right)^{\alpha} \qquad (2)$$

where t_b is the breakthrough time, C_0 is the initial (inlet) concentration of adsorbate (ppmv), α is the constant. Equation (2) predicted the performance of the activated carbon filter.

Yoon and Nelson (**1984**) initially developed a simple model that proposed the rate of decrease in the probability of adsorption for each adsorbate molecule is proportional to the probability of

adsorption of an adsorbate (P_{ads}) and the probability of breakthrough of the adsorbate (1-P_{ads}):

$$\frac{-dP_{ads}}{dt} = k'P_{ads}(1-P_{ads}) \quad (3)$$

Integrating Eq (3), and defining τ as the time required for 50% breakthrough (i.e., P_{ads} = 0.5, hereinafter referred to as the stoichiometric breakthrough time),

$$t_b = \tau + \frac{1}{k'}\ln\frac{C_t}{C_0 - C_t} \quad (4)$$

where k' is a rate constant, C_t is the breakthrough (effluent) concentration of adsorbate. The calculation of theoretical breakthrough curves for a single-component system requires the determination of the parameters *k'* and t for the adsorbate of interest.

In accordance with Eq. (4), the value of k' can be got from the slope of the plot ln [C_t/(C_0 - C_t)] versus breakthrough time *t*, and the value of *t* (50% breakthrough time) can be decided as the time at Q= 0.5 (i.e., $C_t = C_0/2$). Applying k' and *t* of Eq. (4), one may cause the complete breakthrough curve for a given set of experimental conditions. Furthermore, Yoon and Nelson (**1984**) have proposed the following equation:

$$K = k't \quad (5)$$

where *K* is a proportionality constant for a given adsorbate and determined type of adsorbent. Both k' and *t* are alternatively rely on the concentration of the adsorbate and the face velocity.

2.1.3. Kinetic model

The Pseudo-first-order equation is expressed by Lagergren equation (**1898**) as follow:

$$\log(q_e - q_t) = \log q_e - \frac{k_1}{2.303}t \quad (6)$$

where q_e is the amount of adsorbed formaldehyde per unit weight of adsorbent, q_t is the amount of adsorbate adsorbed at time *t*.

The pseudo-second-order model is showed as: (**Ho and McKay, 1999**)

$$\frac{t}{q_t} = \frac{1}{k_2 q_e^{\,2}} + \frac{1}{q_e}t \quad (7)$$

The intraparticle diffusion model is described as follows: (**Guibal, 1998**)

$$q_t = k_i t^{1/2} + C \quad (8)$$

2.1.4. Error analysis

Mandal et al., (2015) used correlation coefficient (R^2) and mean absolute performance error (MAPE) values to verify the experimental data for the most suitable kinetic model**.** These expected indices were computed by utilizing the following equations:

$$R^2 = \frac{[\sum_{i=1}^{n}(q_{pre} - \bar{q}_{pre})(q_{\exp} - \bar{q}_{\exp})]^2}{\sum_{i=1}^{n}(q_{pre} - \bar{q}_{pre})^2 \sum_{i=1}^{n}(q_{ex}p - \bar{q}_{\exp})^2} \quad (9)$$

$$MAPE = \frac{1}{n}\sum_{i=1}^{n}\left|\frac{q_{ex}p - q_{pre}}{q_{\exp}}\right| \times 100 \quad (10)$$

where q_{pre} and q_{exp} are the expected and measured values of formaldehyde concentration, respectively; $\bar{q}$ illustrates the average values of related q; n is the total number of observations.

2.1.5. Adsorption isotherm model

Between adsorbed and free formaldehyde in air, the equilibrium is given by the linearized Langmuir isotherm model as per the following equation (**Bernabe et al., 2015; Cheng and Tsai, 2007**):

$$\frac{C_e}{q_e} = \frac{1}{q_{\max} K_L} + (\frac{1}{q_{\max}})C_e \quad (11)$$

where q_e is the adsorbed amount of formaldehyde per unit weight of adsorbent at equilibrium; C_e is concentration of free formaldehyde in air; q_{max} is maximum adsorption capacity; and K_L is the Langmuir's adsorption equilibrium constant related to the affinity of the binding sites, this phenomena has been described before. (**Bernabe et al., 2015; Cheng and Tsai, 2007**)

Linearized the Freundlich isotherm model is shown as (**Bernabe et al., 2015; Cheng and Tsai,**

2007):

$$\log q_e = \log k_f + 1/n \log C_0 \quad (12)$$

where k_F and n are Freundlich constants, which related to the adsorption intensity and adsorption capacity, respectively. (**Bernabe et al., 2015; Cheng and Tsai, 2007**)

The Dubinin-Radushkevich (D-R) equation, which was initially formulated from the Polanyi adsorption potential theory and represents molecular adsorption as a pore-filling phenomenon rather than a layer-covering one, has been used to correct the Freundlich isotherms (**Yao et al., 2009**). In accordance with the D-R equation the adsorption capacity (W), expressed as the adsorbed liquid volume per unit mass of adsorbent, is related to the adsorption potential (A) as given by (**Dubinin, 1966**)

$$\ln(W / W_0) = -kA^2 \quad (13)$$

and

$$A = RT \ln(P_0 / P) \quad (14)$$

where W is the volumetric adsorption capacity, W_0 is the maximum adsorption space, k is the parameter for each system of adsorbate and adsorbent, A is adsorption potential, R is the universal gas constant, T is the absolute temperature, P_0 is the saturated vapor pressure at temperature T, and P is the partial pressure of the adsorbate. Combined Eqs 13 and 14, the gas-phase partial pressure related to the adsorption capacity as follows

$$\ln W = \ln W_0 - k[RT(P / P_0)]^2 \quad (15)$$

2.2. Experimental methods

The 2.2 mm thickness AC-loaded nonwoven fabric filter media (provided by AIRREX Co. Ltd.) was placed into a 10 cm × 10 cm testing rig located in a a temperature of 28 ±1°C by ambient air-conditioning system. The testing airflow was controlled at relative humidity (RH) of 40 ± 2% by

158 adjusted primary split airflow. The characteristics of fabric filter media and schematic test system
159 diagram are shown in **Table 1** and **Fig. 2**, respectively.

160 **Table 1.** Characteristics of fabric filter media. (**Shiue et al, 2010**)

Raw material	Coconut shell
BET surface area (m^2g^{-1})	1145
Ash content (on dry basis) (%)	3%
Moisture content (%)	20~25%
pHzpc	6
Particle size, mesh	12 × 20 mesh
Thickness, e (mm)	2.2 mm
Weight per surface, W (g m^{-2})	702.8
Specific surface area, SBET (m^2g^{-1})	931.2
Pore volume, Vp (cm^3g^{-1})	0.6762
Microporous volume, Vμp (cm^3g^{-1})	0.3264
Microporous volume percentage, %Vμp (%)	0.48%
Median micropore diameter, dμp	52.08 Å

161 The face velocity of filter media was rated at 0.25, 0.5, and 0.75 m/sec (VT110-VT115
162 Hotwire thermos-anemometer). A source of compressed air was first passed through a drier,
163 adsorbent, and high efficiency particulate air (HEPA) filter to generate a 'zero air'. This zero air
164 was then blended with formaldehyde via a gas-generator to produce the challenge gas entering the
165 test rig (**Fig. 1**). 99.9% grade formaldehyde solvent was filled into the gas-generator and submerged
166 in a water bath (temperature adjustable from 15°C to 25°C). The formaldehyde enters upstream of
167 the testing rig, controlled by passing air through a mass flow controller (Fujikin T1000).
168 Formaldehyde concentration was fixed at 0.25, 0.56 and 0.79 ppm with ±2% deviation. A real-time
169 formaldehyde analyzer (Formaldemeter htv-m) monitored the concentration of the challenge gas.

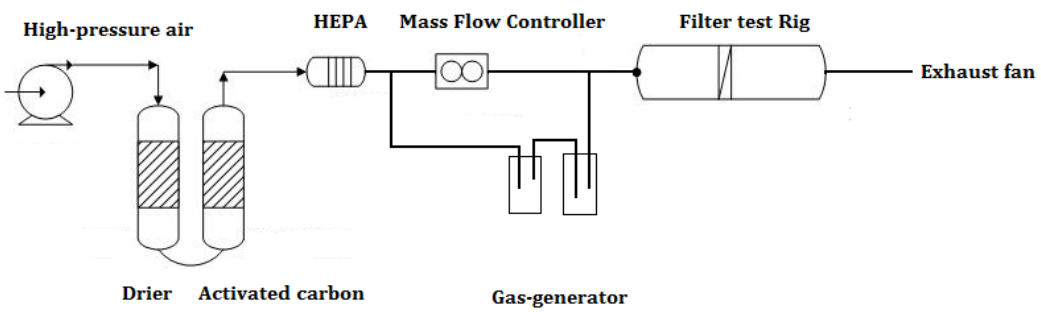

Fig. 2. Schematic diagram of the experimental system setup

2.3. Characterization

Scanning electron microscope (SEM, ZEISS ΣIGMA Essential) was used to study the surface morphology of the adsorbent. X-ray diffraction (XRD) is for chemical characteristics and surface morphology of adsorbent study. Energy-dispersive X-ray spectrometry (EDS, ZEISS ΣIGMA Essential) was employed for the elemental analysis of the sample. To obtain an infrared spectrum of absorption or emission of adsorbnt, Brunauer–Emmett–Teller (BET, Micrometrics ASAP2020) method was used to study the surface area. Fourier-transform infrared spectra (FTIR, Spectrum one) was applied.

3. Results and discussion

3.1. Characterization

3.1.1. Scanning Electron Microscope

Fig. 3 shows the SEM image of AC under different magnification (100, 400, and 2,000) magnification. **Fig. 3(a)** indicated the surface is smooth and distributed with small pores. Moreover, it can observe a little crack and tiny particle near the pore. From **Fig. 3(b)** and **Fig. 3(c)** the surface of AC is rather uneven, coarse and porous. The shape is columnar and lamellar on the surface because the coconuts have the cellulose sintering at high temperature.

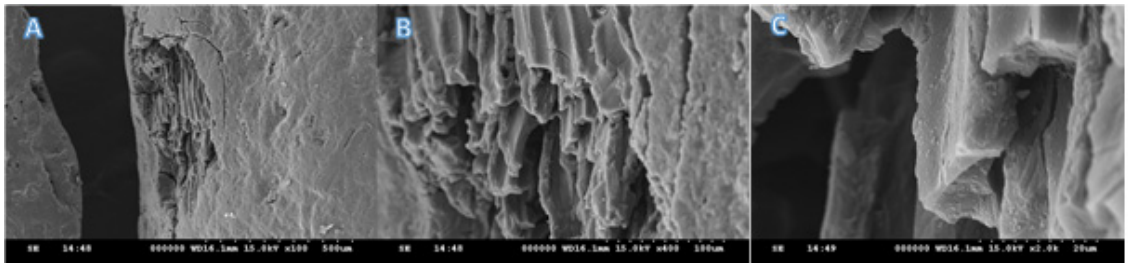

Fig. 3. SEM photographs of AC at (a) 100, (b) 400, (c) 2,000 magnifications.

3.1.2. X-ray diffraction (XRD)

Fig. 4 indicated XRD pattern of AC. The graph was observed that AC is amorphous. The two broad Bragg or diffraction peaks were showed around 22° and 43° indicated that the crystallites were produced by two or more of these plates layer being stacked one above the other. Irregular layer structure were formed the amorphous that the XRD diffraction peaks were broad.

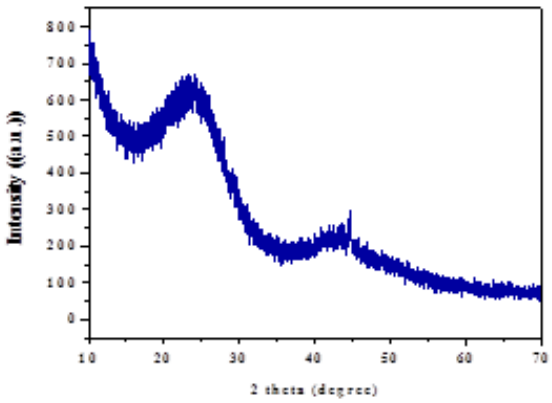

Fig. 4. XRD imagine of AC.

3.1.3. Energy Dispersive X-Ray Spectroscopy (EDS)

Fig. 5 illustrated the EDS detection area of AC, element such as: C, O, Mg, P etc. can be found in the AC. AC is composed of C, O, and P accounting for 77.48%, 18.71%, 3.28% respectively. And we can calculate the O/C ratio= 24.14% which means around 1.0 unit carbons are given by 24.14 unit oxygen. Some metal element like Mg with weight percentage 0.28%. Mg and P are detected in the elemental analysis of AC. The EDS analysis showed that the Mg/C ratio=0.68%, which further

proves the existence of MgO in the coconuts activated carbons.

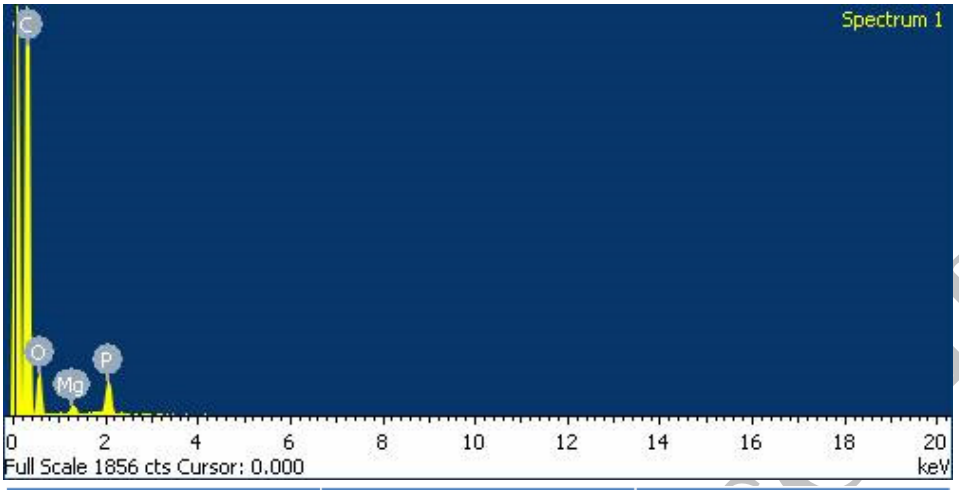

Element	Weight%	Atomic%
C	77.48	83.26
O	18.71	15.09
Mg	0.53	0.28
P	3.28	1.36
Tatals	100.00	

Fig. 5. EDS of AC.

3.1.4. Surface area and pore size

The BET analysis showed that the surface area was 1333.3304 m^2 g^{-1} after BET analysis. The identified data showed that micropore volume of AC is 0.13 cm^3 g^{-1}, meso volume is 0.45 cm^3 g^{-1}, total volume is 0.840442 cm^3 g^{-1}; BJH adsorption average pore diameter is 2.21361nm in the range of 2.0-3.0 nm. The most important thing is the area between adsorption linear and desorption linear in **Fig. 6**.

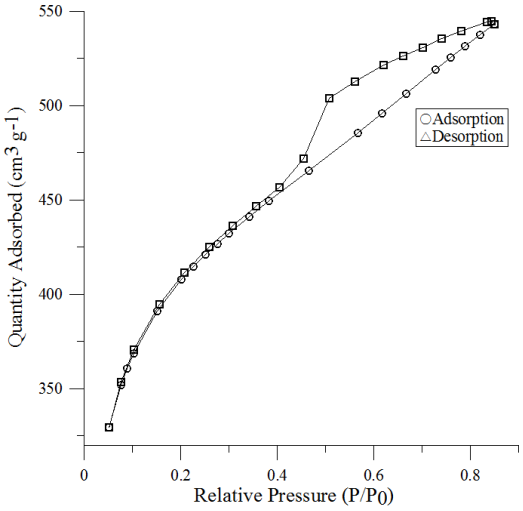

Fig. 6. Adsorption isotherms of N_2 at 77 K on AC.

3.1.5. Fourier Transform Infrared Spectra

Fig. 7 shows FTIR spectroscopy in analysis of the functional groups. AC depended upon the experiments with molecular organic compounds that we can list the orders of the absorptive bands. It showed an intensive band 3417 cm^{-1} has been explained by stretching of ketone -C=O bonds. A weak strength bonding at 2329 cm^{-1} indicated the formation of O-H bonds from carboxylic acid (**Boehm 2002**). Near 1166 and 1086 cm^{-1} has been explained by reverse stretching vibrations of carboxylic acids C-O bonds.

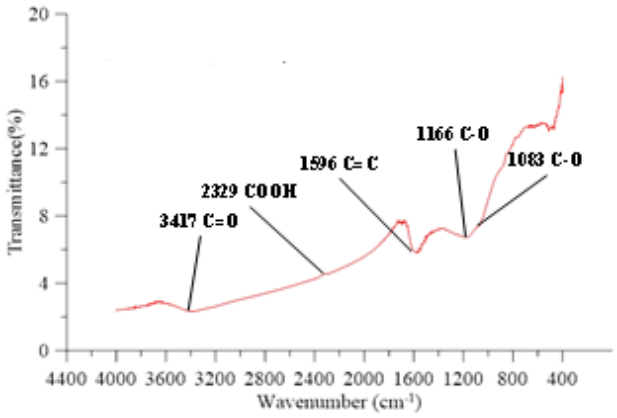

Fig. 7. FTIR imagine of AC.

3.2. Adsorption capacity

Fig. 8 presents variations in formaldehyde adsorption capacity with different inlet concentrations at different face velocities. Equilibrium time (t_t) is defined as the time when the outlet concentration is 98% of the inlet concentration. The proportional relationship between natural logarithm of equilibrium time and formaldehyde adsorption capacity (Q) is presented as the formula (**Scahill et al., 2004**) in **Table 2**. These results are in agreement with **Shiue et al. (2010**) (flow rate of 0.076~0.152 m s^{-1} at an inlet toluene concentration of 10~70 ppm**).** As shown in **Fig. 8**, if the inlet concentration of the adsorbate is increased, resulting in increased velocity of diffusion into the pores of AC, adsorption may reach equilibrium faster; the equilibrium time decreased from 86 to 30 min, 64 to 24 min and 46 to 12 min, while adsorption capacity increased from 0.265 to 0.2991 mg g media^{-1}, 0.3244 to 0.4726 mg g $^{-1}$, and 0.4726 to 0.6019 mg g^{-1} at 0.25, 0.5 and 0.75 m s^{-1} face velocities, respectively.

(a)

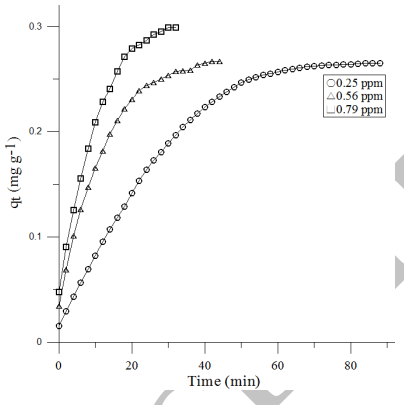

(b)

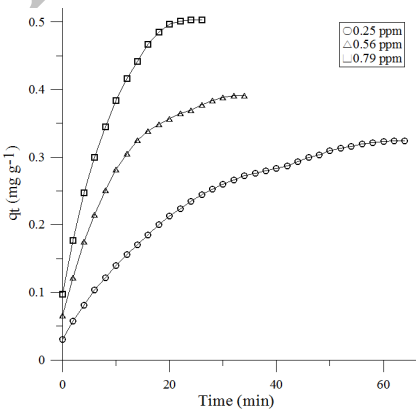

(c)

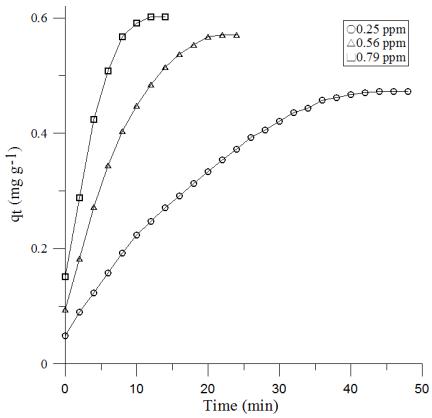

Fig. 8. Effect of concentration on formaldehyde adsorption capacity (a) 0.25m s^{-1}, (b) 0.5 m s^{-1}, (c) 0.75m s^{-1}

Table 2. Correlations of formaldehyde adsorption capacity with time and concentrations.

Face velocity (m s^{-1})	C_i (ppm)	Adsorption capacity (Q) vs time (t)	Adsorption capacity (mg g^{-1})	t (min)
0.25	0.25	$Q = 0.081 \ln(t) - 0.0807$, $R^2 = 0.9596$	0.2650	76
	0.56	$Q = 0.0707 \ln(t) - 0.0098$, $R^2 = 0.9849$	0.2669	41
`	0.79	$Q = 0.0836 \ln(t) - 0.0188$, $R^2 = 0.9861$	0.2989	33
0.5	0.25	$Q = 0.0902 \ln(t) - 0.005$, $R^2 = 0.9785$	0.3244	68
	0.56	$Q = 0.1022 \ln(t) - 0.0441$, $R^2 = 0.9904$	0.3906	38
`	0.79	$Q = 0.1405 \ln(t) - 0.0638$, $R^2 = 0.9873$	0.5029	28
0.75	0.25	$Q = 0.1441 \ln(t) - 0.0815$, $R^2 = 0.9636$	0.4724	44
	0.56	$Q = 0.1695 \ln(t) - 0.0541$, $R^2 = 0.9905$	0.5701	19
`	0.79	$Q = 0.1693 \ln(t) + 0.1882$, $R^2 = 0.9682$	0.6015	12

3.2. Breakthrough

Complete breakthrough is specified as the point at which the measured formaldehyde concentration at the outlet equaled its inlet concentration. Breakthrough was executed by varying initial formaldehyde concentrations from 0.25 to 0.79 ppmv at 0.25 to 0.75 m s^{-1} face velocity shown in **Fig. 9**. The breakthrough time was decreased from 78, 68, and 44 to 34, 28, and 14 min for 0.25 to 0.79 ppmv formaldehyde initial concentrations at 0.25 to 0.75 m s^{-1} face velocity, respectively. This phenomena has been described before (**Jo and Chun, 2014; Cheng and Tsai, 2007**). Additionally, the breakthrough behavior also was decreased from 78, 68, and 34 to 44, 28, and 14 min for 0.25 to 0.75 m s^{-1} face velocity at formaldehyde initial concentration of 0.25, 0.56 and 0.79 ppmv, respectively.

(a) (b)

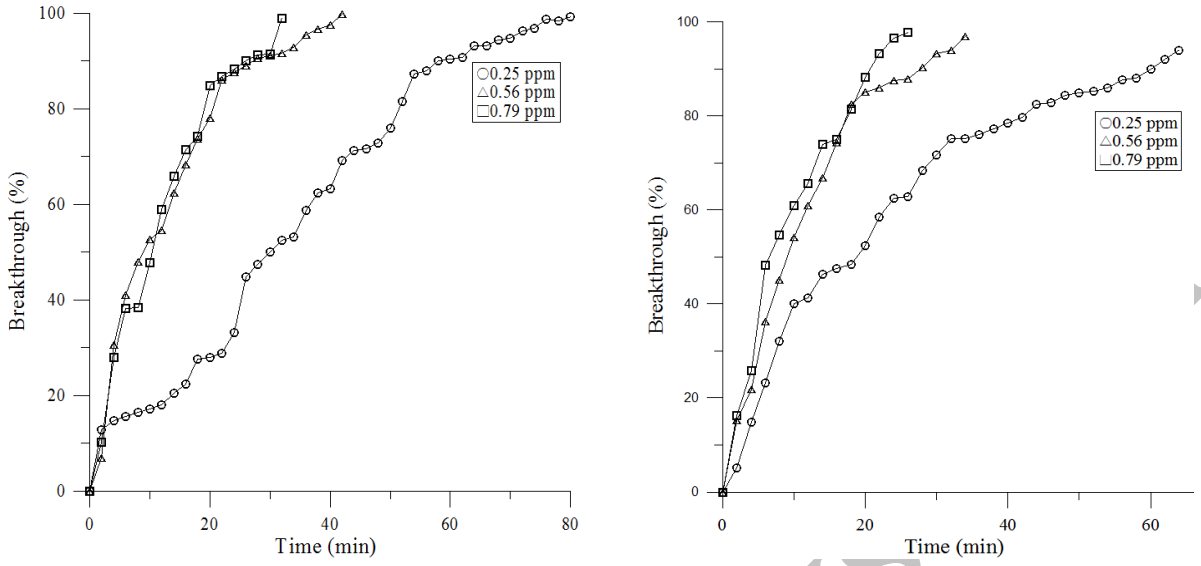

(c)

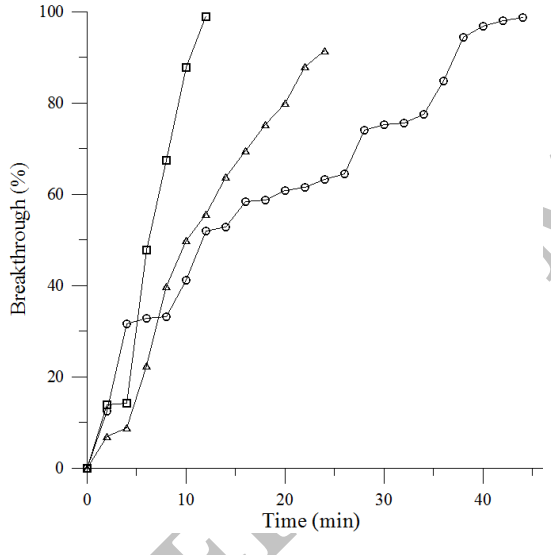

Fig. 9. The breakthrough curves of formaldehyde adsorption at various concentration and various face velocity (a) 0.25 m s^{-1}, (b) 0.5 m s^{-1}, (c) 0.75 m s^{-1}.

The relationships between varies logarithmic formaldehyde initial concentrations and various logarithmic breakthrough times are expressed in **Fig. 10** and **Table 3**. The slopes of the lines were smaller for the formaldehyde with lower face velocity at the same concentration.

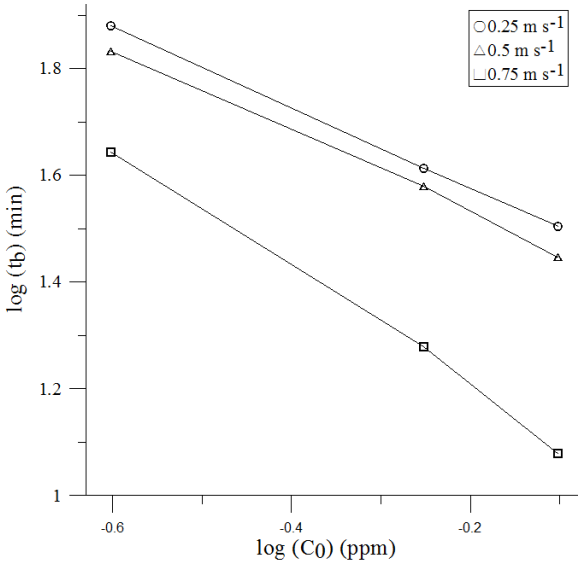

Fig. 10. The relationships between formaldehyde concentrations and breakthrough times.

Table 3. The relationships between formaldehyde concentrations and breakthrough times.

Face velocity (m s^{-1})	Breakthrough time vs Initial concentration
0.25	$t_b C_0^{\,0.1761} = 26.662,\ R^2 = 0.9998$
0.5	$t_b C_0^{\,0.1729} = 23.812,\ R^2 = 0.9975$
0.75	$t_b C_0^{\,0.077} = 9.526,\ R^2 = 0.9963$

The plots of the equation 4 at various face velocities (**Fig. 11**) yielded linear curves with excellent correlations, the end-point of the regression analyses used 50% breakthrough (i.e., $\ln(c_b/c_i - c_b) = 0$). **Table 4** listed the values of the slopes (k') and the intercept of ($-k$). Both k' and τ are dependent on the adsorbate inlet concentration. The rate constant k' increased with increasing formaldehyde inlet concentration, as the stoichiometric breakthrough time τ decreased. Also, both k' and τ were significantly affected by the face velocity; i.e., the value of k' increased with increasing face velocity, while the value of τ decreased. Due to k' and τ act in reverse trend, one would predict that k would be a constant with a well-behaved breakthrough times presented in **Fig. 11**. Certainly, as interpreted in **Table 4**, the value of proportionality constant K (2.60 ± 0.47)

277 could be utilized as a basis of prevision for other hypothetical formaldehyde concentrations and face

278 velocities.

279 (a) (b)

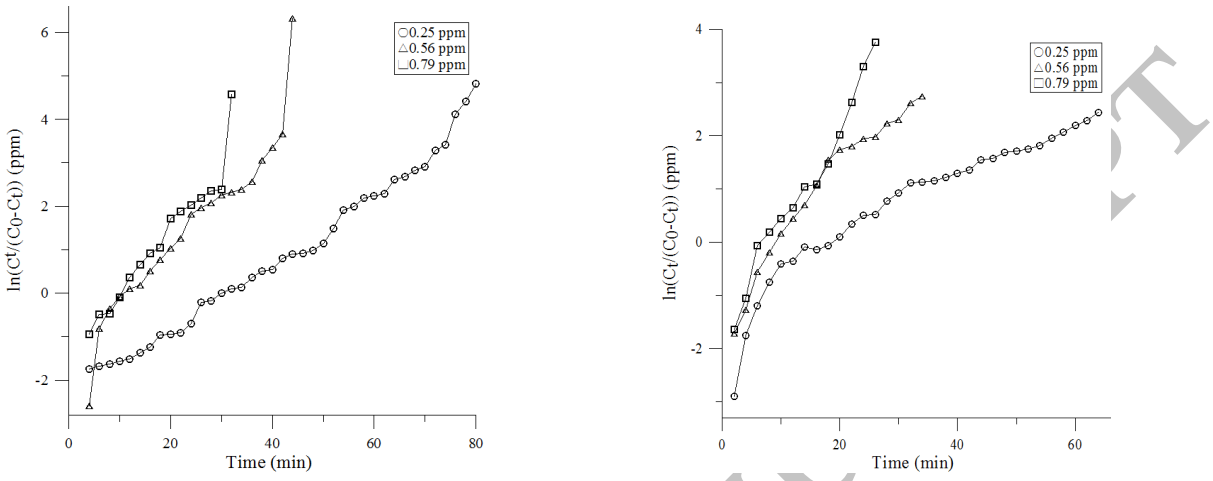

280

281 (c)

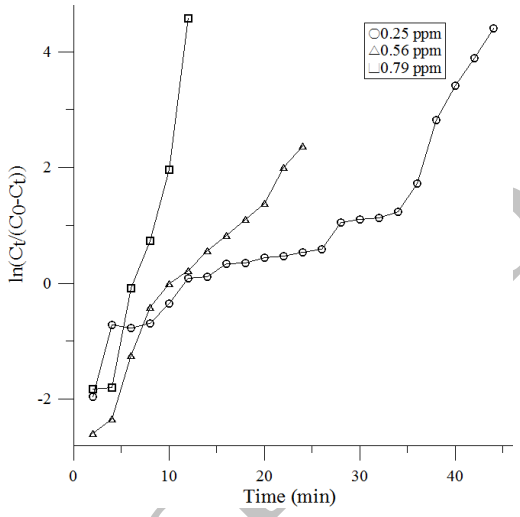

282

283 **Fig. 11**. Effect of concentration on ln[(C_i-C_b)/C_b] (a) 0.25m s^{-1}, (b) 0.5 m s^{-1}, (c) 0.75m s^{-1}

284 **Table 4.** The theoretical parameters $k't$, and K

Face velocity (m s^{-1})	Concentration (ppm)	k' (min^{-1})	t(min)	K	R^2
0.25	0.25	0.081	40	3.232	0.981
	0.56	0.124	22	2.737	0.978
	0.79	0.143	16	2.294	0.972
0.5	0.25	0.056	32	1.792	0.973
	0.56	0.183	17	3.114	0.972
	0.79	0.201	13	2.613	0.972

0.75	0.25	0.086	22	1.892	0.973
	0.56	0.197	12	2.359	0.979
	0.79	0.565	6	3.389	0.972

285 **3.3. Adsorption kinetic models**

286 To determine the sorption mechanism, three common kinetic models, Pseudo-first-order,
287 Pseudo-second-order, and intra-particle diffusion models were applied to empirically analyze
288 kinetic sorption data.

289 ***3.3.1. Pseudo-first-order model***

290 The plot of Pseudo-first order kinetics is shown in **Fig. 12**. **Table 4** summarized the calculated
291 constants according to the Pseudo-first-order equation along with correlation coefficients (r_1^2). The
292 adsorption amount $q_{e,1}$ of formaldehyde increased from 0.264, 0.324, and 0.472 to 0.298, 0.502, and
293 0.601 mg g^{-1} for 0.25 to 0.79 ppmv formaldehyde initial concentrations at 0.25 to 0.75 m/sec face
294 velocity, respectively. It shows formaldehyde removal efficiency is dependent on initial
295 concentration. In addition, the amount of formaldehyde adsorption decreased from 0.571, 0.787,
296 and 0.986 to 0.291, 0.441, and 0.820 mg g $media^{-1}$ for 0.25 to 0.75 m s^{-1} face velocity at 0.25, 0.56
297 and 0.79 ppmv formaldehyde initial concentration, respectively. The removal efficiency of
298 formaldehyde is also dependent on face velocity. Moreover, the calculated data of $q_{e,1}$ are closer to
299 the experimental data. With the initial concentration increased from 0.25 to 0.79 ppm at face
300 velocity 0.25 to 0.75 m s^{-1}, the rate constant (k_1) values were increased from 0.77 to 0.145, 0.082 to
301 0.227 and 0.125 to 0.547 min^{-1}, respectively. The rate constant (k_1) of the pseudo-first-order rate
302 model is linearly related to formaldehyde initial concentration (C_0) is shown in **Fig. 13**. This result
303 is similar to the findings of many previous studies (**Saeid and Bahare, 2006**).
304
305
306

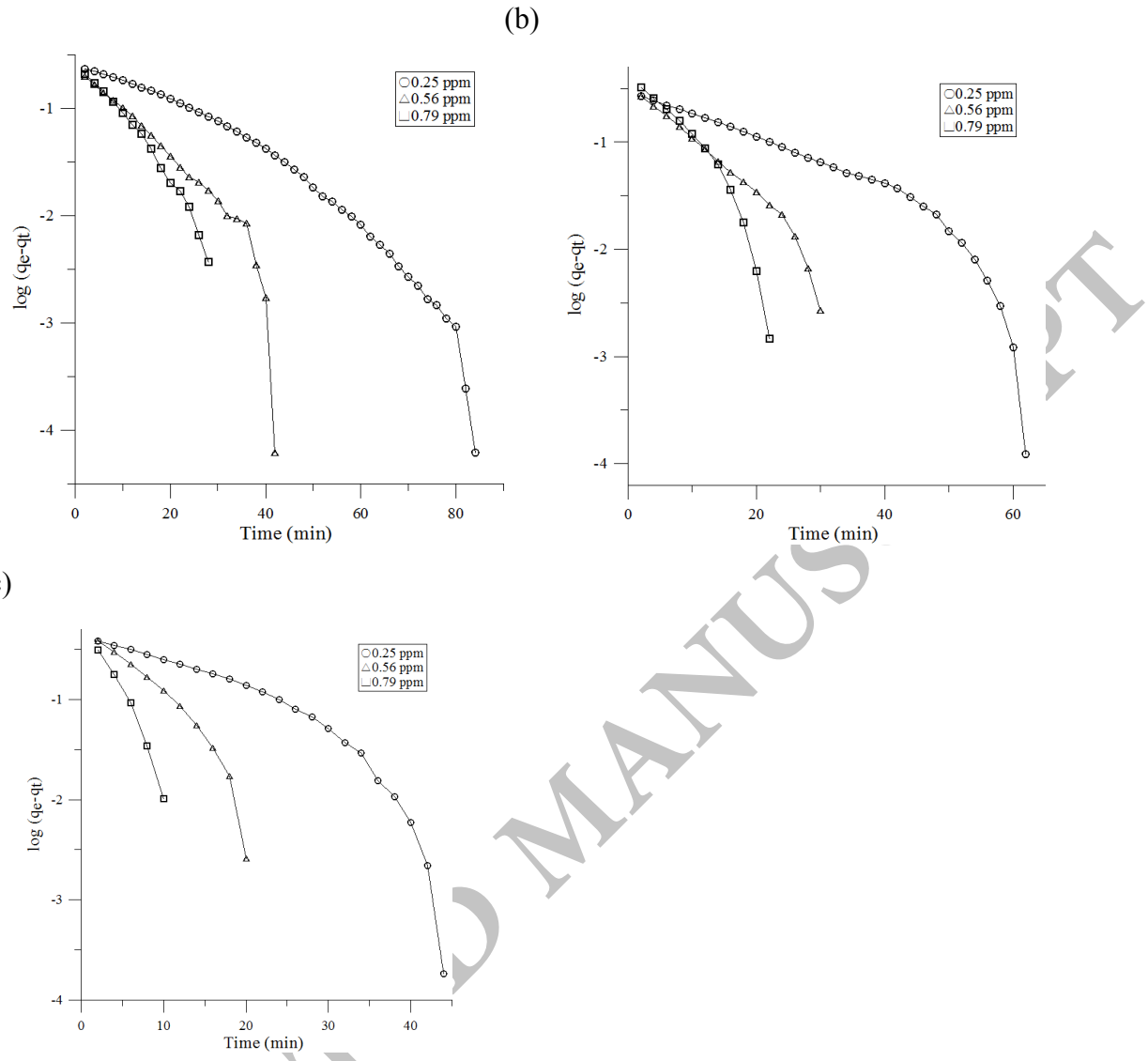

Fig. 12. Plot of Pseudo-first order kinetics at face velocity (a) 0.25 m s^{-1}, (b) 0.5 m s^{-1}, (c) 0.75 m s^{-1}.

Table 4. Fitting parameters of three kinetic models for formaldehyde adsorption.

Face velocity	Inlet concentration	Pseudo-first-order				Pseudo-second order				Intraparticle diffusion			
		k_1(min^{-1})	$q_{e,1}$ (mg g^{-1})	r_1^2	MAPE (%)	k_2 (g mg^{-1} min^{-1})	$q_{e,2}$ (mg g^{-1})	r_2^2	MAPE (%)	k i (mg g^{-1} $min^{-1/2}$)	C	r_i^2	MAPE (%)
0.25 m s^{-1}	0.25 ppm	0.077	0.571	0.915	161.51	0.323	0.309	0.96	5.49	0.031	0.019	0.846	12.43
	0.56 ppm	0.108	0.349	0.969	14.96	0.683	0.329	0.984	2.35	0.037	0.053	0.813	7.89
	0.79 ppm	0.145	0.291	0.977	25.27	0.715	0.35	0.973	4.63	0.049	0.057	0.867	6.4
0.5 s^{-1}	0.25 ppm	0.082	0.787	0.803	88.69	0.4	0.402	0.972	3.92	0.041	0.048	0.895	6.69
	0.56 ppm	0.142	0.548	0.959	20.69	0.689	0.436	0.983	3.67	0.06	0.087	0.832	6.57
	0.79 ppm	0.227	0.441	0.896	119.21	0.716	0.522	0.972	5.46	0.089	0.11	0.871	5.67

	0.25 ppm	0.125	0.986	0.795	156.27	0.409	0.498	0.94	5.94	0.072	0.055	0.924	8.72
0.75 m s^{-1}	0.56 ppm	0.225	0.825	0.896	64.36	0.705	0.785	0.965	6.12	0.109	0.103	0.876	7.06
	0.79 ppm	0.547	0.82	0.878	66.19	0.721	0.919	0.974	7.92	0.133	0.153	0.843	5.93

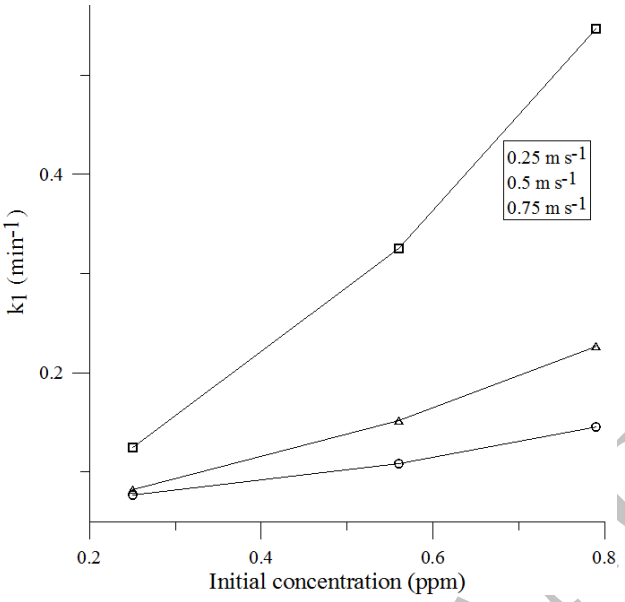

Fig. 13. The relationship between the Pseudo-first-order rate constant and formaldehyde initial concentration.

3.3.2. Pseudo-second-order model

Fig. 13 presents a plot of the Pseudo-second order kinetics for the formaldehyde adsorption onto AC filter media**. Table 4** summarizes the calculated constants (k_2) of the Pseudo-second-order equation along with correlation coefficients (r_2^2). The adsorption amount ($q_{e,2}$) of the formaldehyde increased from 0.309, 0.329, and 0.715 to 0.498, 0.785, and 0.721 mg g^{-1}media^{-1} for 0.25 to 0.79 ppmv formaldehyde initial concentrations at 0.25 to 0.75 m/sec face velocity, respectively. The formaldehyde removal is based on initial concentration. In addition, the amount of formaldehyde adsorption $q_{e,2}$ increased from 0.309, 0.402, and 0.498 to 0.35, 0.522, and 0.919 mg g^{-1}media^{-1} for 0.25 to 0.75 m/sec face velocity at 0.25, 0.56 and 0.79 ppmv formaldehyde initial concentration, respectively. It shows that the formaldehyde removal efficiency is also dependent on face velocity. With initial concentration increased from 0.25 to 0.79 ppm at face velocity 0.25 to and 0.75 m s^{-1}, the rate constant (k_2) values were increased from 0.323, 0.4, and 0.409 to 0.715, 0.716, and 0.721 g

mg^{-1} min^{-1}, respectively. Moreover, the calculated $q_{e,2}$ values are closer to the experimental data, the rate constant (k_2) of the pseudo-second-order rate model related to formaldehyde initial concentration (C_0) is shown in **Fig. 14**. This result is similar to the findings of many previous studies (**Saeid and Bahare, 2006**).

(a) (b)

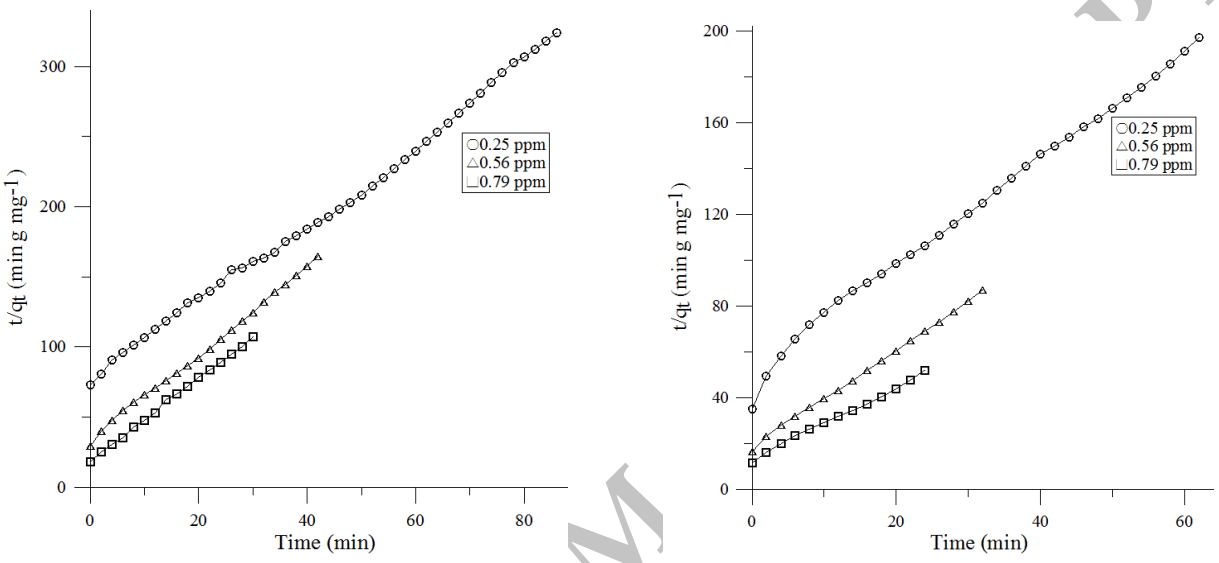

(c)

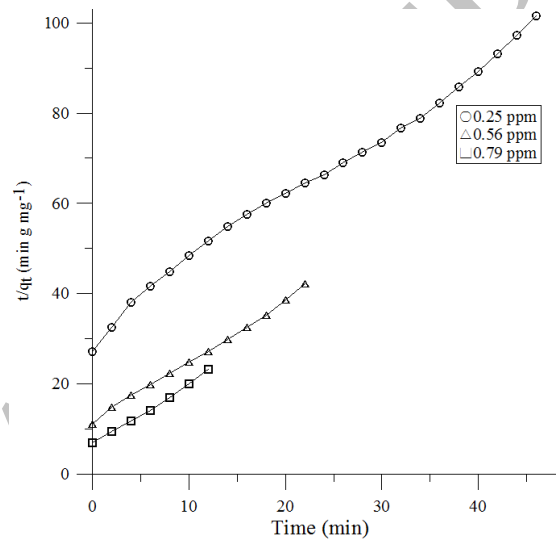

Fig. 13. Plot of Pseudo-second order kinetic for the adsorption of formaldehyde at face velocity (a) 0.25 m s^{-1}, (b) 0.5 m s^{-1}, (c) 0.75 m s^{-1}.

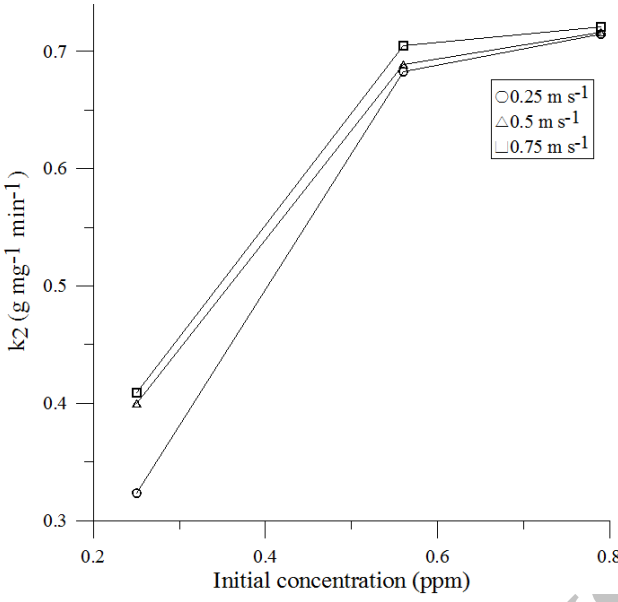

Fig. 14. The relationship between the Pseudo-second-order rate constant and formaldehyde initial concentration.

3.3.3. Intraparticle diffusion model

Fig. 15 shows the plot of intraparticle diffusion model. The rate constants (k_i) are obtained from the slope of the line on second stage. C value of the intercept demonstrated some degree boundary layer thickness. It is larger to promote the greater effect of the boundary layer. k_i and C value with its correlation coefficients are shown in **Table 4**. The adsorption process presented three steps: stage 1: the adsorbate molecules diffused in the adsorption and adsorbed on the outer surface (**Shiue and Hu 2012; Tang et al. 2016; Hu et al., 2017; Shiue et al. 2017**). Stage 1 is finished before 2 min. average at 0.25 to 0.79 ppm inlet formaldehyde concentrations of 0.25, 0.5, and 0.75 m s^{-1} face velocity, respectively. Stage 2: this stage is a developed process and k_i is the highest, resulting that the intraparticle diffusion is the key controlling factor of adsorption rate. (**Shiue and Hu 2012; Tang et al. 2016; Hu et al., 2017; Shiue et al. 2017**) It kept and continues from 2 min to 25~49, 16~36, and 9~25 mins of AC adsorptive filter media at 0.25 to 0.79 ppm inlet concentration of 0.25, 0.5, and 0.75 m s^{-1} face velocities, respectively. Stage 3: this stage is the adsorption equilibrium process, where the intraparticle diffusion further slows down, and the adsorption rate

decreases significantly due to the adsorbates almost filled the micropores and mesopores. (**Shiue and Hu 2012; Tang et al. 2016; Hu et al., 2017; Shiue et al. 2017**) It starts after the above mentioned time schedule at 0.25 to 0.79 ppm inlet formaldehyde concentration of 0.25, 0.5, and 0.75 m s^{-1} face velocity, respectively. The formaldehyde is slowly removed via intraparticle diffusion into the particles and is finally kept in the micropores. Generally, intraparticle diffusion rate constant k_i is the slope of the stage 2 line. The values of k_i arise from 0.031 to 0.049 $min^{-1/2}$ (0.25m s^{-1}), from 0.041 to 0.089 $min^{-1/2}$ (0.5m s^{-1}), and from 0.072 to 0.133 $min^{-1/2}$(0.75m s^{-1}) of AC adsorptive filter media when increase from 0.25ppm to 0.79ppm, respectively. Nevertheless, the linear intercept C is not zero and larger, showing that the membrane diffusion in stage 3 also affected the adsorption rate. (**Tang et al. 2016**) Three stage of the intraparticle diffusion model fitted the adsorption data well. The formaldehyde adsorption onto AC adsorptive filter media is affected by combined intraparticle diffusion model and membrane diffusion (**Tang et al. 2016**).

(a) (b)

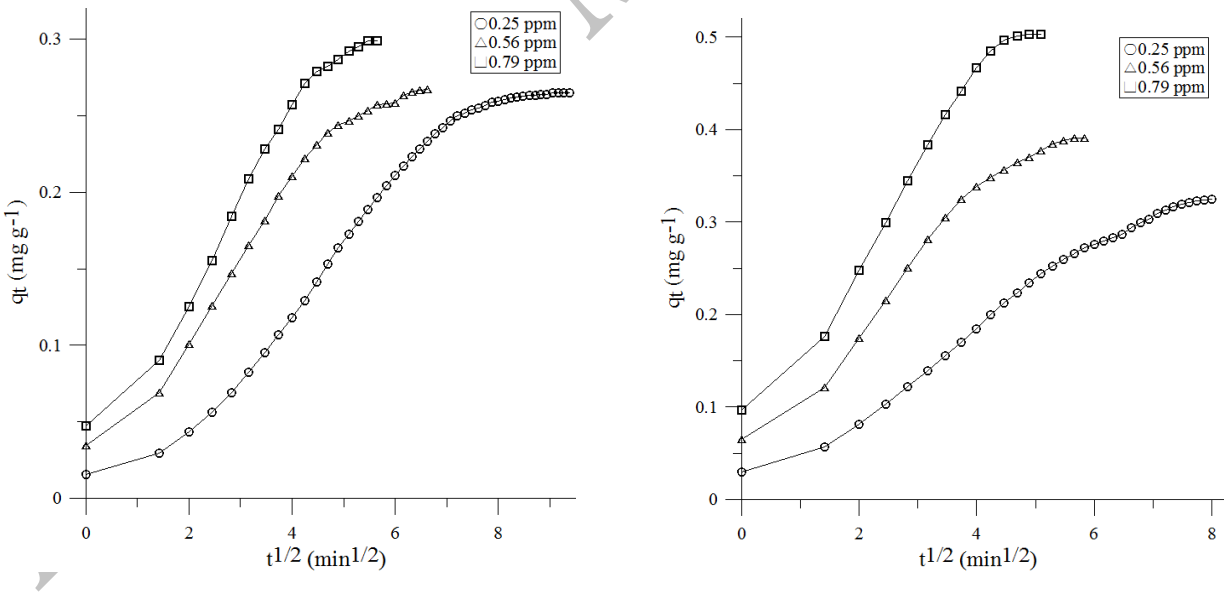

(c)

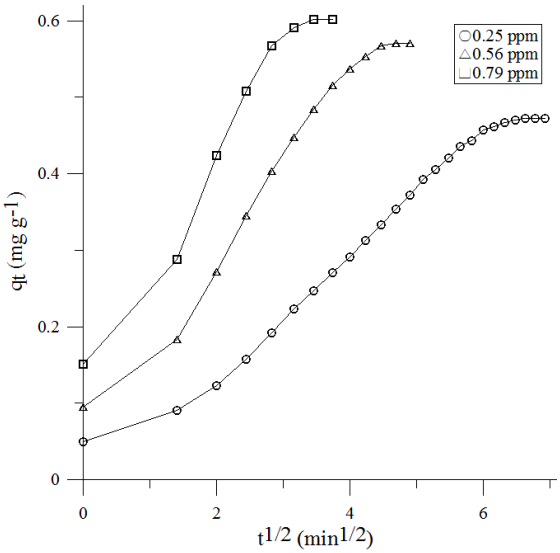

Fig. 15. Plot of intraparticle diffusion model at face velocity (a) 0.25 m s^{-1}, (b) 0.5 m s^{-1}, (c) 0.75 m s^{-1}.

3.3.4. Error Analysis

The correlation coefficients of the Pseudo-second order kinetic model (Average value = 0.969) is higher than the Pseudo-first order kinetic model (Average value = 0.899) and the intraparticle diffusion model (Average value = 0.863). This result is similar to the findings by Tsai et al. (2017) and Adelodun et al. **(2016).** For the adsorption process, physisorption might be the controlling mechanism by the highest correlation coefficient (Average value = 0.969) and the lowest mean absolute percentage error value (Average MAPE <8%) verification. Only the intraparticle diffusion model fits the experimental data. Thus, it was determined to be the rate limiting step for the initial period of the adsorption process.

3.4. Adsorption isotherms

The plots of the Freundlich and Langmuir isotherm models are presented as **Figs. 16** and **17**, respectively. The isotherm constants and maximum adsorption capacity (q_{max}) values are listed in **Table 5**. According to the linear regression method, the formaldehyde adsorption by AC adsorptive filter media exhibits a better fit to Langmuir equation was statistically confirmed by giving

greater R^2 values closer to unity (R^2 >0.987). This denotes that the Langmuir model may better describe an adsorption isotherm for AC adsorptive filter media. This adsorptive behavior pointed out that the adsorption occurs on a heterogeneous surface, which may be aspect to the various active sites on AC adsorptive filter media. The overall adsorptive performance is prevailed as a physical adsorption process. This phenomena has been described before (**Bernabe et al., 2015; Cheng and Tsai, 2007**). The results show that the maximum formaldehyde adsorption capacity (q_{max}) of AC adsorptive filter media was 0.7862 mg g^{-1} at 0.75m s^{-1} face velocity. From the observed results we conclude that AC adsorptive filter media is potentially a good solution for formaldehyde removal.

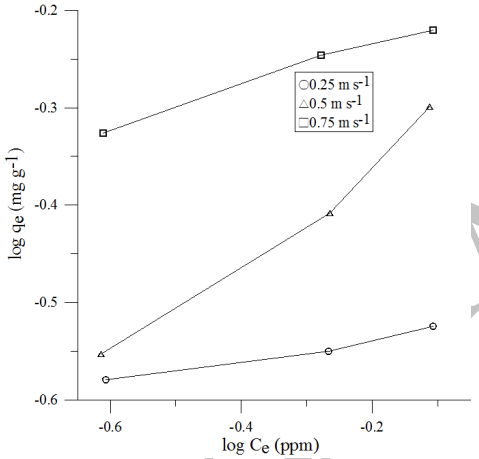

Fig. 16. Formaldehyde adsorption with Freundlich adsorption isotherm.

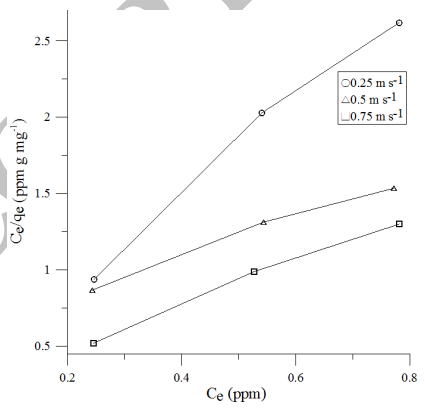

Fig. 17. Formaldehyde adsorption with Langmuir adsorption isotherm.

406 **Table 5.** Freundlich and Langmuir isotherm parameters

Face velocity	Freundlich isotherm			Langmuir isotherm		
($m\ s^{-1}$)	K_f ($mg\ g^{-1}$)($L\ mg^{-1}$)$^{1/n}$	1/n	R^2	q_{max}($mg\ g^{-1}$)	K_L ($L\ mg^{-1}$)	R^2
0.25	0.5965	0.1061	0.9738	0.3167	15.2046	0.9872
0.5	0.6121	0.2133	0.9794	0.6864	8.058	0.9879
0.75	0.8242	0.4908	0.9886	0.7862	2.2	0.9923

407 Except than the Freundlich and Langmuir isotherms, the experimental data were also
408 represented by the D–R equation. **Fig. 18** was plotted as lnW versus A^2 for AC filter from
409 adsorption isotherms of N_2 data of **Fig. 3**. As shown in the figure, the characteristic curve for
410 formaldehyde is simulated linearly at a lower A^2 range. Nevertheless, the isotherm data of
411 formaldehyde cannot be linearly fitted over the entire range of abscissa. A clear transition was
412 observed at ~2.2 x 10^7 $J^2\ mol^{-2}$ of A^2, which is equal to a relative pressure (P/Po) of 0.151 for the
413 adsorbates to represent a good fit at lower levels of A^2 (high P/Po) and of a big discrepancy at high
414 A^2 (low P/Po) in agreement with Shiue et al. (**2011**) research work. The results show that the D–R
415 equation can simulate the experimental adsorption data except very low relative pressures. In the
416 event of relative pressures lower than 0.151, the D–R equation may be difficult to utilize the
417 simulation of the adsorption capacity for the tested adsorption systems.

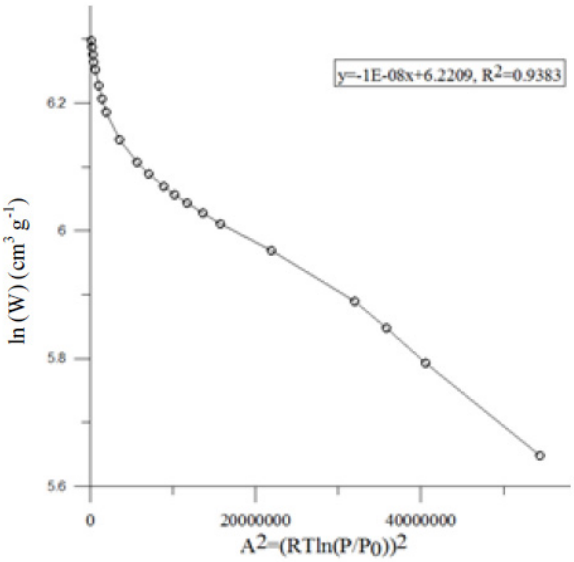

418

419 **Fig. 18.** The D-R isotherm

4. Conclusions

This study concludes that formaldehyde removal byAC adsorptive filter media is effective in the indoor environment. From SEM images it was found the micrographs show that AC surface is smooth and distributed with small pores. The surface of AC is rather uneven, coarse and porous. Irregular layer structure were formed the amorphous that the XRD diffraction peaks were broad. In EDS analysis C, O, Mg, P etc. were detected, which showed that the Mg/C ratio=0.68% and further proves the existence of MgO in AC. Therefore, the surface area is 1333.3304 $m^2 g^{-1}$ according to BET analysis by checking with FTIR, ketone -C=O bonds which is explained at sensible peak of 3417 cm^{-1} and weak strength bonding at 2329 cm^{-1} were successfully grafted on carbon.

The results presented that increased initial concentration of formaldehyde and face velocity were associated with a higher adsorption capacity and faster breakthrough time. The breakthrough behavior at low formaldehyde concentration can be linearly expressed by the relationship between the natural logarithm of breakthrough time and the natural logarithm of initial concentration. It is proved that the agreement between the Yoon and Nelson model and the experimental data is high due to high correlation coefficients (R^2>0.972) for formaldehyde adsorption onto coconut activated carbon filter media. For adsorption kinetics of formaldehyde removal by AC adsorptive filter media, the Pseudo-second-order model with highest correlation coefficient ($0.94 < R^2 < 0.984$) and lowest MAPE values (8 %) is more suitable than Pseudo-first-order-model, and intraparticle diffusion model and membrane diffusion could predict the adsorption kinetics. The Langmuir equations is well-fitted to AC adsorptive filter. The D–R equation successfully predicted the equilibrium capacity of formaldehyde onto AC at high relative pressures. The overestimation of adsorption capacity was detected when seeking to expect the formaldehyde adsorption capacity at relative pressures 0.151.

Acknowledgements

The authors would like to acknowledge the supports from the Ministry of Science and Technology with contract number 105-3011-F-027-001.

Nomenclature

C intercept of intraparticle diffusion model, mg kg^{-1}

Ce concentration of free formaldehyde in air, ppm

C_0 the inlet concentration, ppm

k_1 the pseudo-first-order rate coefficient, min^{-1}

k_2 the pseudo-second-order rate coefficient, g mg^{-1} min^{-1}

k_i the intraparticle diffusion rate constant, mg g^{-1} $min^{-1/2}$

K_L the Langmuir's adsorption equilibrium constant related to the affinity of the binding sites, L mg^{-1}

q_e the amount of adsorbed formaldehyde per unit weight of adsorbent, mg g^{-1}

q_{max} maximum adsorption capacity, mg g^{-1}

q_t the amount of adsorbate adsorbed at time t, mg g^{-1}

t testing time, min

V the airflow rate, L min^{-1}

References

Adelodun, A.A., Ngila, J.C., Kim, D.G., Jo, Y.M. (2016). Isotherm, Thermodynamic and Kinetic Studies of Selective CO_2 adsorption on Chemically Modified Carbon Surfaces. Aerosol and Air Quali. Res. 16: 3312–3329.

Bernabe, D.P., Herrera, R.A.S., Doma Jr., B.T., Fu, M.L., Dong, Y.C., Ya-Fen Wang, Y.F. (2015). Adsorption of Low Concentration Formaldehyde in Air Using Ethylene-Diamine Modified

467 Diatomaceous Earth. Aerosol and Air Quali. Res. 15: 1652–1661.
468 Boehm HP (2002) Surface oxides on carbon and their analysis: a critical assessment. Carbon 40(2):
469 145-149.
470 Bolis, V. (2013). Fundamentals in Adsorption at the Solid-Gas Interface. Concepts and
471 Thermodynamics. Calorimetry and Thermal Methods in Catalysis. Chapter 1: 3-50.
472 Brunsgaard, C., Heiselberg, P., Knudstrup, M.A., Larsen, T.S. (2012). Evaluation of the indoor
473 environment of comfort houses: qualitative and quantitative approaches. Indoor Built Environ
474 21(3): 432–451.
475 Cheng, W.H. (2008). Adsorption Characteristics of Granular Activated Carbon and SPME
476 Indication of VOCs Breakthrough. Aerosol and Air Quali. Res. 8(2): 178-187.
477 Cheng, W.H., Tsai, S.C. (2007). Competition among Mixed Adsorbates Affecting the Adsorption of
478 Gaseous Methyl Ethyl Ketone by Hydrophobic Molecular Sieve. Aerosol and Air Quali. Res.
479 7(2): 205-220.
480 Chuck, W.F., Kim, J.T. (2013). Photocatalytic Oxidation for Maintenance of Indoor Environmental
481 Quality. Indoor Built Environ. 22(1): 39–51.
482 Danielle, C., Joao, Luiz A.D., Vitor, R. da S., Luciana, I.M., Marcos, R.M. (2013). Adsorption of
483 volatile aroma compound 2-phenylethanol from synthetic solution onto granular activated
484 carbon in batch and continuous modes. J. of Food Engineer. 117: 370–377
485 Dehdashti A, Khavanin A, Rezaee A, Assilian H, Motalebi M (2011) Application of microwave
486 irradiation for the treatment of adsorbed volatile organic com-pounds on granular activated
487 carbon. Iran. J. Environ. Health. Sci. Eng. 8: 85–94.
488 Dubinin, M.M. (1966). Chemistry and Physics of Carbon; Walker, P.L., Ed.; Marcel Dekker: New
489 York, NY, Vol. 2, 51-120.
490 Gilbert NL, Guay M, Gauvin D, Dietz RN, Chan CC, Levesque B (2008) Air change rate and
491 concentration of formaldehyde in residential indoor air. Atmos Environ 42(10): 2424-2428.

492 Guibal, E. (1998). Metal-Anion Sorption by Chitosan Beads: Equilibrium and Kinetic Studies.
493 Indus. and Eng. Chem. Res. 37: 1454-1463.
494 Ho, Y.S., McKay, G. (1998). The kinetics of sorption of basic dyes from aqueous solution by
495 sphagnum moss peat. Canadian J. of Chem. Eng. 76: 822-827.
496 Jo, W.K., Chun, H.H. (2014). Application of Fibrous Activated Carbon Filter in Continuous-Flow
497 Unit for Removal of Volatile Organic Compounds under Simulated Indoor Conditions. Aerosol
498 and Air Quali. Res. 14: 347–354.
499 Lagergren, S. (1898). Zur theorie der sogenannten adsorption gelo¨ sterstoffe, Kungliga Svenska
500 Vetenskapsakademiens. Handling. 24 (4): 1-39.
501 Liang, W., Li, J., Jin, Y. (2012). Photo-catalytic degradation of gaseous formaldehyde by TiO_2/UV,
502 Ag/TiO_2/UV and Ce/TiO_2/UV. Build and Environ. 51: 345- 350.
503 Lu, N., Pei, J.J., Zhao, Y.X., Qi, R.Y., Liu, J.J. (2012). Performance of a biological degradation
504 method for indoor formaldehyde removal. Building and Environ. 57: 253- 258.
505 Lu, C.L., Pan, L.W., Zhu, B. (2015). Study the Static Adsorption-Desorption of Formaldehyde on
506 Activated Carbons. International Forum on Energy. Environ. Sci. and Materials 943-947.
507 Mandal, S., Mahapatra, S.S., Adhikari, S., Patel, R.K. (2015). Modeling of Arsenic (III) Removal
508 by Evolutionary Genetic Programming and Least Square Support Vector Machine Models.
509 Environ. Process 2: 145–172
510 Malina, J. and A. Rađenović, A. (2014). Kinetic Aspects of Methylene Blue Adsorption on Blast
511 Furnace Sludge. Chem. Biochem. Eng. Q. 28 (4): 491–498.
512 Mui, K.W., Wong, L.T., Hui, P.S. (2008). Policy influence of formaldehyde exposure risk in air-
513 conditioned office environment. Indoor Built Environ. 17(5): 449–454.
514 Rengga, W.D.P., Sudibandriyo, M., Mohammad Nasikin, M. (2016). Adsorptive Removal of
515 Formaldehyde by Chemically Bamboo Activated Carbon with addition of Ag nanoparticle:
516 Equilibrium and Kinetic. MATEC Web of Conferences 5: 04004.

517 Saeid, A., Bahare, Y. (2006). Adsorption of 18-crown-6 from aqueous solution on granular
518 activated carbon: A kinetic modeling study. J. of Coll. and Inter. Sci. 299: 112–115.
519 Scahill J, Wolfrum EJ, Michener WE, Bergmann M, Blake DM, Watt AS (2004) A New Method
520 for the Rapid Determination of Volatile Organic Compound Breakthrough Times for a Sorbent
521 at Concentrations Relevant to Indoor Air Quality. J. of Air & Waste Manage. Assoc. 54:
522 105–110.
523 Shiue, A., Hu, S.C. (2012). Adsorption Kinetics for the Chemical Filters Used in the make-up air
524 unit (MAU) of a cleanroom. Separa. Sci. and Techn 47: 577–583.
525 Shiue, A., Den, W., Kang, Y.H., Hu, S.C., Jou, G.T., Lin, C.H., Hu, M.C., Lin, S.I. (2011).
526 Validation and Application of Adsorption Breakthrough Models for the Chemical Filters Used
527 in the make-up air unit (MAU) of a cleanroom. Building and Environ. 46(2): 468- 477.
528 Shiue, A., Kang, Y.H., Hu, S.C., Jou, G.T., Lin, C.H., Hu, M.C., Lin, S.I. (2010). Vapor adsorption
529 characteristics of toluene in an activated carbon adsorbent-loaded nonwoven fabric media for
530 chemical filters applied to cleanrooms. Building and Environ. 45(10): 2123-2131.
531 Tsai, C.Y., Chiu, C.H., Chuang, M.W., His, H.C. (2017). Influences of Copper(II) Chloride
532 Impregnation on Activated Carbon for Low-Concentration Elemental Mercury Adsorption
533 from Simulated Coal Combustion Flue Gas. Aerosol and Air Quali. Res. 17: 1637–1648.
534 U.S. Consumer Product Safety Commission. (2015). An updated on formaldehyde.
535 Vimonses V, Lei S, Jin B, Chow C.W.K., Saint C (2009) Kinetic study and equilibrium isotherm
536 analysis of Congo Red adsorption by clay materials. Chem. Eng. J. 148: 354–364.
537 VanOsdell D.W., Owen M.K., Jaffe L.B., Sparks L.E. (1996) VOC removal at low contaminant
538 concentrations using granular activated carbon. J. Air Waste Manag. Assoc. 46: 883–890.
539 Wang, Z.Q., Pei, J.J., Jensen, S., Zhang, J.S. (2014). Experimental investigation of the
540 formaldehyde removal mechanisms in a dynamic botanical filtration system for indoor air
541 purification. J Hazard Mater. 280: 235-243.

542 Yao, M., Zheng, Q., Hand, D.W., Perram, L. (2009). Investigation of the Treatability of the Primary
543 Indoor Volatile Organic Compounds on Activated Carbon Fiber Cloths at Typical Indoor
544 Concentrations. Journal of the Air & Waste Management Association 59(7): 882-890.
545 Ye, J.J., Ye, F., Dai, W., Ding, D. (2015). Formaldehyde Capture with Finger Citron Residue Based
546 Activated Carbon. Separation Sci. and Techn. 50: 253–259.
547 Yu, C.W.F., Kim, J.T. (2010). Building pathology, investigation of sick buildings – VOC emissions.
548 Indoor Built Environ. 19(1): 30–39.